NAFEMS Conference
2008
United Kingdom

3D MODELLING OF A WIND TURBINE USING CFD

David Hartwanger[*] and Dr Andrej Horvat[†]

[*] Intelligent Fluid Solutions (South Africa)
david.hartwanger@intelligentfluidsolutions.co.uk

[†] Intelligent Fluid Solutions (United Kingdom)
andrej.horvat@intelligentfluidsolutions.co.uk

Key words: CFD, Wind Turbine, Efficiency

Abstract
Turbine efficiency remains a critical component of the overall economic justification for a potential wind farm. There is therefore a requirement for prediction methodologies that are capable of addressing the in-situ performance of multiple turbine installations within a specific local environment and operating in a range of conditions. The work presented here is the first stage in a programme of work that aims to develop a practical engineering methodology for the CFD-based assessment of multiple turbine installations. In this first stage a CFD benchmarking exercise was performed using the wind turbine design in the Unsteady Aerodynamics Experiment (UAE) conducted by the US National Renewable Energy Laboratory. Initially blade sections were analysed in 2D and the results used to construct and validate a 3D CFD model of the turbine. The 3D results were used to develop estimates for actuator disk induction factors. Finally these factors were used to modify the classical actuator disk treatment of wind turbines. The results from the modified actuator disk model were in good agreement both with CFD and experiment.

1.0 Maximum Ideal Efficiency
The ideal, frictionless efficiency of a wind turbine was predicted by A. Betz in 1920 using a simple one-dimensional model. The rotor is represented by an "actuator disk" that creates a pressure discontinuity of area A and local velocity V [1, 2]. The control volume of the model is defined by a stream tube whose fluid passes through the rotor disk. The wind at the inlet to the model has an approach velocity V_0 over an area A_0, and a slower downstream velocity V_3 over a larger area A_3 at the outlet. A simple schematic of the model is given in Figure 1.

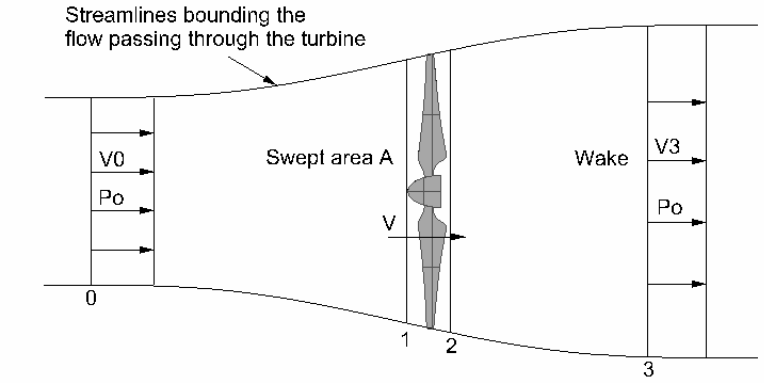

Figure 1. Control volume for the idealised actuator-disk analysis

The actuator disc approach uses the following assumptions:

(1) The flow is ideal and rectilinear across the turbine i.e. steady, homogenous, inviscid, irrotational, and incompressible.
(2) Both the flow and thrust are uniform across the disk.
(3) The static pressure at the upwind and downwind boundaries is equal to the ambient static pressure.

The wind exerts an axial thrust, T on the turbine in the flow direction. An equal and opposite force is exerted by the turbine on the wind through its mounting with the ground. By applying a horizontal momentum relation between sections *0* and *3* the thrust at the rotor disk can be found:

$$\sum F_x = -T = \dot{m}(V_0 - V_3) = rAV(V_0 - V_3) \tag{1}$$

where *?* is the density of the air. The thrust at the turbine is also the differential pressure between stations *1* and *2* multiplied by the disk area:

$$T = (p_1 - p_2)A \tag{2}$$

It can be shown that the pressures, p_1 and p_2, can be obtained by applying Bernoulli's equation to portions of the control volume upstream and downstream of the turbine where no work is done. Therefore:

$$p_1 - p_2 = \frac{1}{2} r \left(V_0^2 - V_3^2\right) \tag{3}$$

Substituting this result into (2) and equating with (1) yields:

$$V = \frac{1}{2}(V_0 + V_3) \tag{4}$$

where V is the stream velocity at the turbine.

Continuity and momentum therefore require that the velocity V through the disk equal the average of the wind speed and the downstream wake velocity. The fractional decrease in wind velocity between the free stream and rotor plane can be expressed in terms of an axial induction factor, a:

$$a = \frac{V_0 - V}{V_0} \tag{5}$$

The maximum value of a = ½, since this requires V_3 to reduce to zero. Substituting a into the above relations, the thrust at the turbine disk can be written as:

$$T = \frac{1}{2} rAV_0^2 4a(1-a) \tag{6}$$

The power coefficient, C_p, defined as the extracted power over the total available power can similarly be defined in terms of a as:

$$C_p = 4a(1-a)^2 \tag{7}$$

Figure 2 plots equation 7 and shows that C_p reaches a maximum value of 0.593 when a = ? . The corresponding downstream wake velocity, V_3 = ? V_0 and the wake area A_3 is double the turbine swept area. This is known as the Betz limit for an ideal frictionless turbine. This model is independent of turbine rotational speed, and requires a uniform pressure distribution over the disk area. In reality a real wind turbine does not achieve this efficiency level due to:

(1) Rotation in the wake caused by the reaction with the spinning rotor
(2) A non-uniform pressure distribution in the turbine plane
(3) Aerodynamic drag due to viscous effects.
(4) Energy loss due to vortices at the blade tips

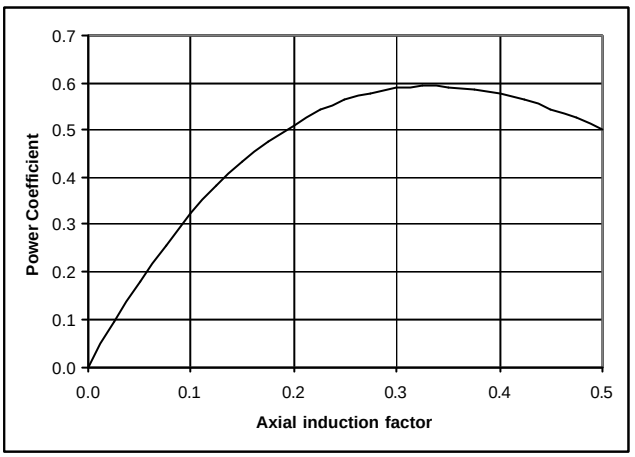

Figure 2. Power Coefficient for an ideal Betz model wind turbine

The impact of the rotating wake (1) can be estimated by extending the Betz analysis to a 2-D model in the radial direction. The control volume in Figure 1 is divided into many non-interacting annular stream tubes, so that all the previous variables can be functions of the annular radius.

The flow far upstream is purely axial; however there is a discontinuous jump in angular velocity across the rotor plane because torque is exerted on the rotor. The turbine wake rotates in the opposite direction to the rotor with an angular velocity, ? at the rotor plane, which is considered to be the average of ?$_1$ and ?$_2$. Two additional expressions are customarily introduced: an angular induction factor, a', and a local speed ratio, ?$_r$, defined as:

$$a' = \frac{w_2}{2\Omega} \tag{8}$$

$$l_r = \frac{\Omega r}{V_0} \tag{9}$$

In 1935 H. Glauert derived the expression for the pressure, $p_1 - p_2$, when the angular component of velocity is taken into account, by applying an energy balance across the rotor plane [2, 3]:

$$p_1 - p_2 = r\left(\Omega + \tfrac{1}{2}w_2\right)w_2 r^2 \tag{10}$$

Where O is the angular velocity of the turbine and r is the radius of the annular stream tube at the rotor plane. By applying the conservation of angular momentum the resulting differential

thrust and torque on an annular ring of the disk, expressed in terms of the induction factors are:

$$dT = r\Omega^2 r^2 4a'(1+a')\rho r dr \tag{11}$$

$$dTo = r V_0 \Omega r^2 4a'(1-a)\rho r dr \tag{12}$$

Also, it can be shown for an ideal turbine the two induction factors are related. Equation 6 for the thrust across the rotor disk can be expressed in terms of the turbine radius and equated with equation 11. Introducing the local speed ratio, $?_r$, and solving for *a'* the following relationship can be derived:

$$a' = \frac{1}{2}\left(\sqrt{1+\frac{4}{l_r^2}a(1-a)}-1\right) \tag{13}$$

For an ideal turbine operating at maximum efficiency $a = ?$, constant over the swept area, while *a'* decreases with increasing local speed ratio. Figure 3 shows the calculated maximum theoretical efficiency taking wake rotation into consideration. The figure also confirms that turbines with high tip speed and low angular induction factor are able to deliver better efficiency.

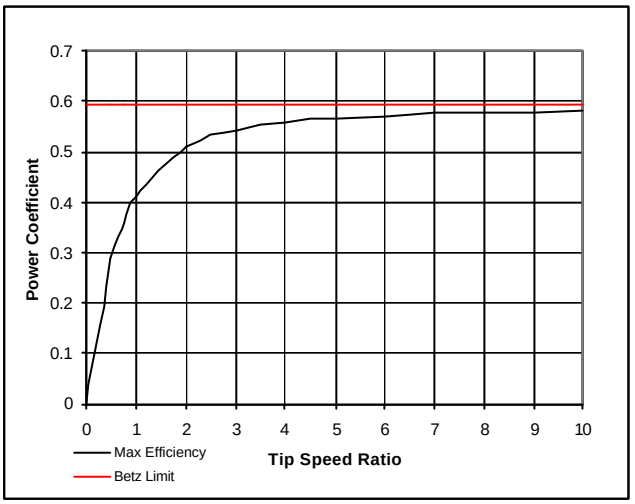

Figure 3. Theoretical maximum power coefficient

Glauert's wake rotation model is still subject to the assumptions of a uniform pressure distribution and zero radial velocity in the turbine plane (as in the Betz analysis). These assumptions lead to an overestimation of the forces and torque applied to the turbine. Therefore, Glauert's model asymptotes towards the Betz limit as the tip-speed ratio tends to infinity, i.e. as the rotation in the wake tends to zero.

More recently, in 2001, Gorban, Gorlov and Silantyev [4] introduced an alternative (GGS) model, that considers non-uniform pressure distribution and curvilinear flow across the turbine plane (two of the other practical issues not included in the Betz approach). The curvilinear flow refers specifically to the diverging streamlines across the turbine plane, rather than rotation in the wake about the turbine axis. The GGS model is shown in figure 4.

The principal assumption of the GGS model is that the flow crosses the turbine plane at the same angle at any point. This angle has been defined as the pitch angle, f, (shown in figure 4). The angle of f depends upon the permeability of the turbine plane. If the turbine is

considered as a semi-penetrable obstacle for the flow with a certain resistance density *r*, then the filtration equation holds:

$$-\left(\frac{dp}{dx},\frac{dp}{dy},\frac{dp}{dz}\right)=r\left(V_x,V_y,V_z\right) \tag{14}$$

Therefore, the power extracted by the turbine is given by:

$$P=\int \nabla p\cdot V=\int r\left|V\right|^2 \tag{15}$$

which is solved for vectors normal to the turbine plane. Therefore when $r = 0$, there is full filtration and f = p/2 or when $r = 8$ there is no filtration and f = 0. The velocity and pressure distribution can be solved using a modified Kirchhoff flow analysis, for a given pitch angle.

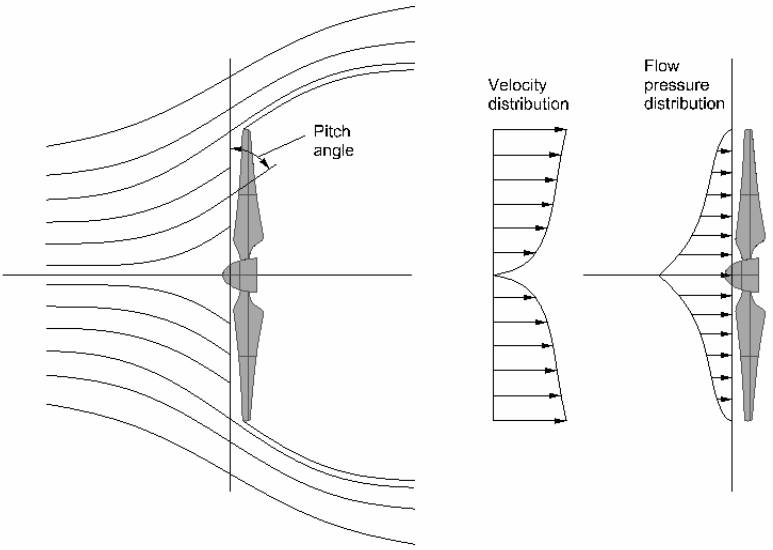

Figure 4. GGS curvilinear flow model in incompressible flow

The efficiency, obtained by dividing equation (15) by the power carried by the flow passing through the turbine swept area, can be optimized with respect to the pitch angle. Furthermore, for a given turbine filtration, the flow passing through the swept area can be expressed as a fraction of the free stream at infinity. This definition is not restricted by the wake velocity, as in the Betz analysis, but can vary from 0 for no filtration to 1 for full filtration. The efficiency and Flow through predicted by the GGS model is given in figure 5.

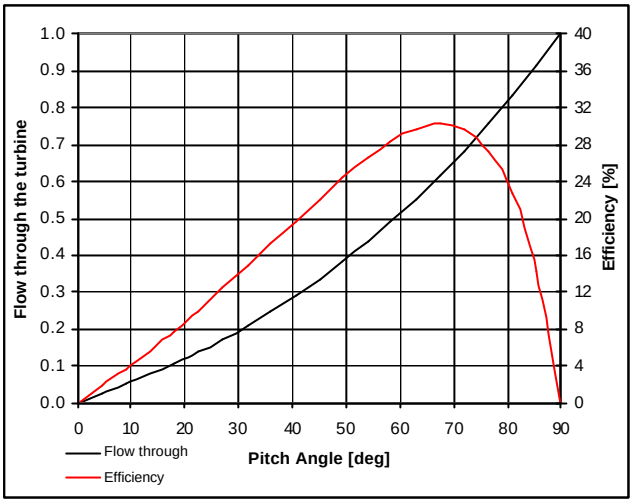

Figure 5. Efficiency and Flow through versus the pitch angle

The model predicts a peak efficiency of 30.1% at f = 67.5^0 and a flow through of 0.613. This is substantially more conservative than either the Betz or Glauert models. The GGS model predicts that peak efficiency is achieved when the flow through the turbine is approximately 61% which is very similar to the Betz result of 2/3rd. A comparison between the two models is plotted in figure 6.

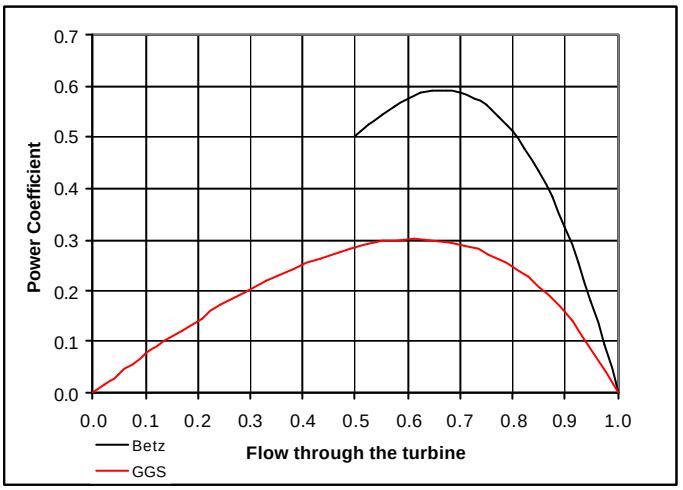

Figure 6. Power Coefficient versus Flow through the turbine

Although real wind turbines do not attain the levels predicted by Betz or Glauert they do achieve and exceed the level predicted by Gorlov et al. Therefore, we can conclude that the Glauert model is optimistic, while the GGS model is conservative and highly efficient real turbines possibly lie somewhere in between.

The empirical models suggest that for a wind turbine to attain near ideal efficiency it should exhibit the following characteristics:

(1) Relatively low resistance to the flow, allowing approximately 65% of the stream to pass through.
(2) High tip-speed ratios so that the angular momentum in the wake is low.

2.0 Performance of Real Wind Turbines

The performance of real wind turbines is limited by the following factors:

(1) Non-uniform pressure and turbulence distribution over the swept area.
(2) Angular momentum in the wake.
(3) Blade tip losses as a result of tip vortices.
(4) Aerodynamic drag and boundary layer separation due to viscous related effects.

Figure 7 shows a comparison of real turbine performance and the ideal maximum according to Glauert. The V52/850 is a 3-bladed Vestas turbine 52m in diameter with a rated power output of 850 kW. The turbine rotor speed is 20 rpm at peak efficiency, resulting in a tip speed ratio of 6.7 and delivers power coefficients greater than 0.45 for wind speeds ranging from 6 to 10 m/s. The blade pitch is variable, controlled by a microprocessor-based monitoring system. This turbine is therefore representative of current state of the art technology and capability.

The UAE turbine is a full-scale experimental turbine designed and built by the US Department of Energy's National Renewable Energy Laboratory (NREL) to specifically advance the current understanding and prediction of wind turbine performance [5]. For accurate and reliable test data NREL constructed a comprehensive test program known as the Unsteady Aerodynamics Experiment (UAE). The unit is a 2-bladed, 10m diameter, 20 kW wind turbine and was tested at the NASA-Ames Research Centre Wind Tunnel.

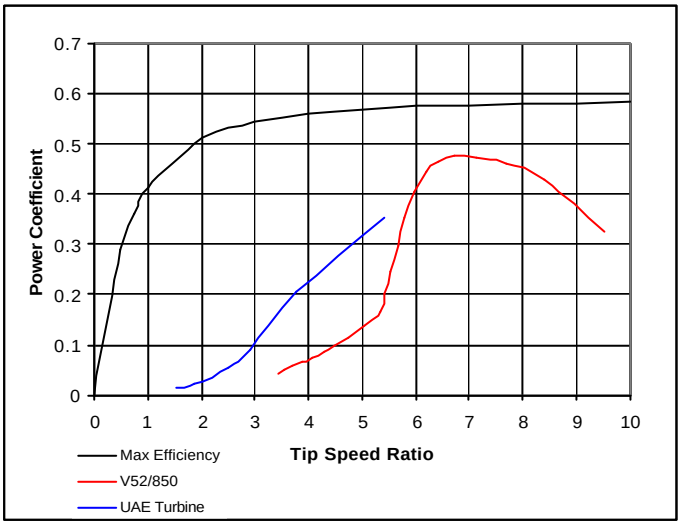

Figure 7. Typical turbine performance from real devices

The UAE turbine achieves a peak efficiency of approximately 36% at a tip speed ratio of approximately 5.5 in the controlled wind tunnel environment. This corresponds to a wind speed of 6.9 m/s and a rotor speed of 72 rpm. The performance of the turbine in a real environment varies from the wind tunnel results, mainly due to the local turbulence variations in the atmospheric boundary layer [6]. However, the primary aim of the UAE turbine was to assist the advancement of numerical design tools for the wind power industry.

The experimental data from the UAE turbine makes it possible to gain a deeper insight into the factors limiting current wind turbines, in relation to the simple actuator disk theory. Furthermore, the experimental database has allowed extensive validation of predictive codes, including CFD (Computational Fluid Dynamic) techniques.

3.0 CFD Analysis of S809 Aerodynamic Characteristics

Wind turbine design relies on accurate aerodynamic aerofoil data over the full design space. Errors in the performance coefficients will result in errors in the turbine's performance estimates and corresponding economic projections. Extensive experimental data including the lift, drag and moment coefficients are usually required for detailed design. However, this is not always available in which case numerical calculations must be relied upon. A range of numerical tools are available including commercial CFD codes that are considered very accurate for attached flow. However, CFD models tend to exhibit poor predictive performance in the post stall operating range [7].

The UAE turbine was selected for a 3D CFD validation exercise, which was preceded however, by a 2D aerofoil section analysis. The turbine was designed using the S809 aerofoil section throughout the blade length, (see figure 8). Results from 2D experiments [1] were compared with the results from the XFOIL 6.0 panel code, and two CFD ANSYS-CFX analyses. The primary aim of this phase of the programme was to asses the general predictive accuracy of the numerical tools in terms of the 2D lift and drag polar. A secondary aim was to assess the relative difference between a high fidelity CFD model and a lower fidelity more practical model, to serve as a guide for the 3D analyses to be performed in the next stage of the programme. Typically a high resolution structured grid with advanced turbulence and transition modeling is required for 3D wind turbines. However, this places a high demand on computational power and time [8]. Therefore, the lower fidelity CFD model was investigated in order to assess the potential loss in predictive accuracy. Table 1 summarises the essential features of the CFD models and the results are shown in figure 9.

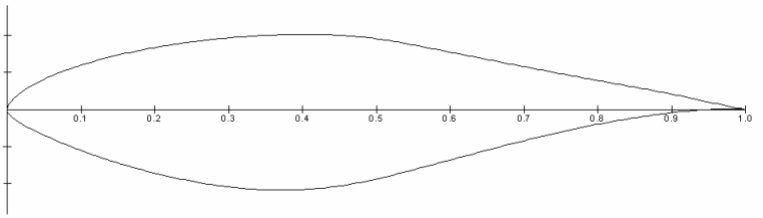

Figure 8. S809 Aerofoil section

Table 1. Normal and High Fidelity CFD models

	Normal Fidelity (CFD-NF)	High Fidelity (CFD-HF)
Domain size (L = chord length)	10L × 10L	10L × 10L
No. of nodes	22,110	75,600
Trailing Edge	Blunt (modified)	Sharp
Turbulence model	k-epsilon	Shear Stress Transport
Laminar-turbulence transition	No	Yes
y-plus	~ 30	~ 1

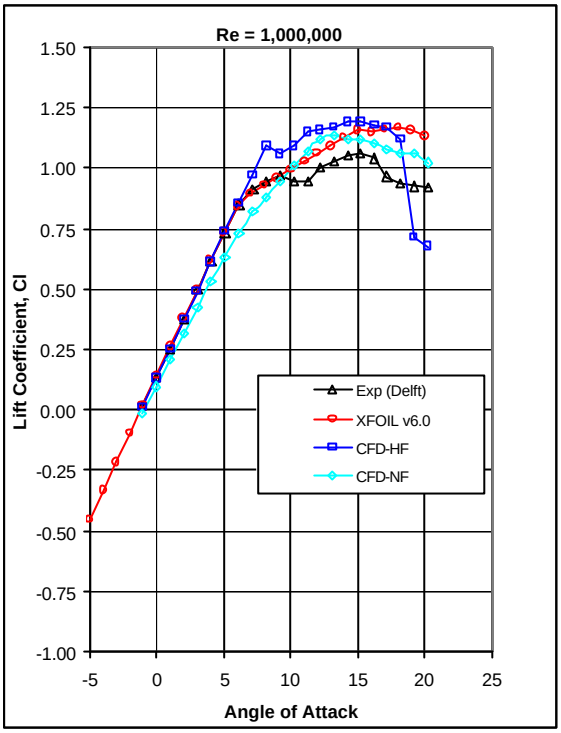

Fig 9a: Lift Coefficient

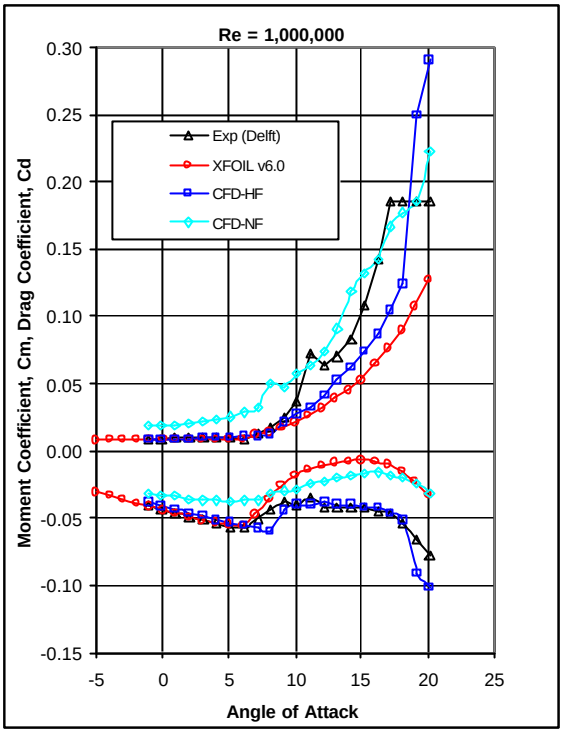

Fig 9b: Moment and Drag Coefficients

Figure 9. 2D lift, drag and moment measurements

The normal fidelity CFD model was constructed using an unstructured grid of wedge elements. Three inflation layers were used to resolve the near wall boundary. Furthermore, the trailing edge of the aerofoil was truncated to provide a 1.65% blunt edge thickness. This was applied to improve the robustness of the meshing tool and mesh quality. The high fidelity model was constructed using a structured grid of hexahedral elements, with approximately 20 nodes placed within the boundary layer thickness. The aerofoil trailing edge was un-modified, i.e. sharp trailing edge was retained. Table 2 shows a comparison of the percentage differences between the three numerical models and the experimental data.

Table 2. Percentage error of numerical models

a	Lift Coefficient			Drag Coefficient			Moment Coefficient		
	XFOIL	CFD-NF	CFD-HF	XFOIL	CFD-NF	CFD-HF	XFOIL	CFD-NF	CFD-HF
1.02	3.5	-18.5	-1.6	-4.3	105.0	-3.5	0.5	-26.2	-6.1
5.13	1.6	-13.8	0.4	-9.9	164.7	5.2	-2.2	-33.3	-4.5
10.2	5.2	6.7	14.9	-39.3	52.9	-26.8	-56.5	-27.2	1.2
15.23	8.8	5.1	12.6	-48.5	21.6	-31.4	-83.4	-60.4	-0.8

The high fidelity CFD model and XFOIL are in good agreement with experiment up to an angle of attack of 6^0, i.e. while the flow is attached. At higher angles of attack these two approaches over-predict the lift and under-predict the drag, possibly due to under-predicting boundary layer separation. The normal fidelity CFD model demonstrates the worst accuracy in the attached flow regime, but comparable performance with the other two models in the stalled flow regime.

Based upon the results in Table 2 one may conclude that the high-fidelity CFD model would be most suitable for high tip-speed ratios (>3), while tending to over-predict performance at

low tip-speed ratios (<2). The normal fidelity model is likely to under-predict performance at high tip-speed ratios.

4.0 CFD Analysis of the UAE Wind Turbine

CFD modeling of the UAE wind turbine was performed using ANSYS-CFX 11.0 in conjunction with ANSYS ICEMCFD meshing tool. The geometry of the turbine was constructed in Rhinoceros (see Figure 10) from detailed specifications of local section profile, chord length and twist angle [1]. The blade was designed using the NREL S809 aerofoil shape over the complete length. Blade pitch is fixed and power is regulated using stall control at the tips.

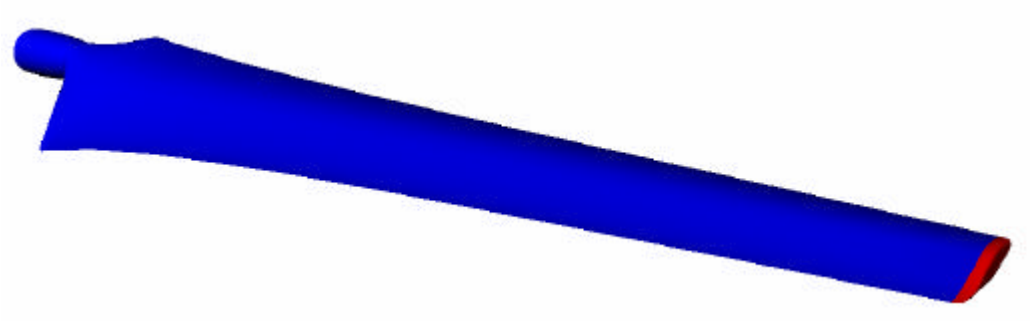

Figure 10. UAE turbine blade constructed in Rhinoceros CAD

The turbine was placed in a cylindrical domain of radius 2L and length 5L (L = turbine radius). The upstream boundary was positioned 2L from the turbine. A full 360^0 model was constructed, consisting of a local disk of unstructured mesh containing the turbine rotor, and a background structured mesh (Figure 11). The local disk containing the turbine was 1m wide and 5.2m in radius. The disk region contained 1.15 million numerical nodes, whilst the background mesh contained 264,000 nodes. Three inflation layers were applied over the blade surface with sufficient resolution for the k-epsilon turbulence model. A coarse resolution equivalent to the 2D case was applied in conjunction with a blunt trailing edge.

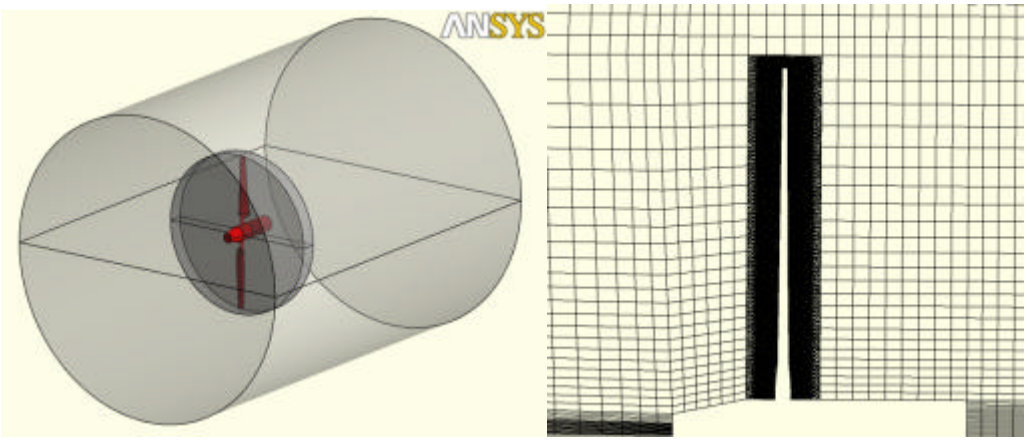

Figure 11. CFD 3D model and mesh construction

A steady state solution was obtained using the CFX Frozen-rotor model, and a local timescale factor of 1. A total pressure inlet boundary condition was applied with static pressure downstream boundary and domain perimeter. Converged solutions were obtained after approximately 1000 iterations.

Figures 12 and 13 show a reasonably good match of torque and power between the CFD model and the NREL experimental results. At low wind speeds (TSR > 3) the CFD model under-predicts the turbine performance. Since the majority of the blade surface is operating within the attached flow regime, based upon the 2D results, the CFD model is under-predicting lift and over-predicting drag. However, in the separated flow regime the CFD model tends to over-predict performance due to an over-prediction of the aerodynamic lift

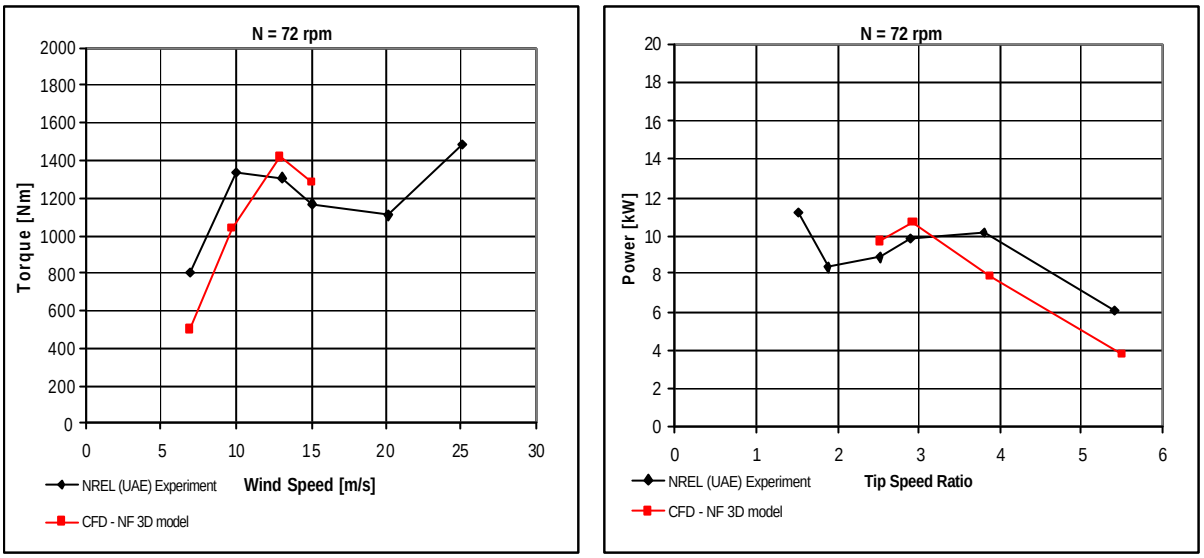

(a) Measured Torque Output (b) Measured Power output

Figure 12. Results comparison between CFD and experiment

The results from the CFD analysis of the UAE turbine were used to determine the axial and angular induction factors for classical actuator model. The results were used to construct an equivalent actuator disk model of the UAE turbine.

5.0 An Equivalent Actuator Disk Model

Representing a real turbine with an equivalent actuator disk in a 3D CFD model offers a potentially economically viable analysis tool for assessing turbine response in a range of conditions and environments [9]. The 3D UAE turbine CFD results were used to estimate the axial and angular induction factors for populating the momentum equations (11) and (12) from the classic actuator disk theory. These two expressions represent the momentum loss and source, for the thrust and torque respectively within a permeable finite volume representing the turbine.

The actuator disk model relies upon averaged effects over the swept area of the turbine. Therefore, velocity and pressure data were sampled from two planes just upstream and downstream of the UAE turbine, as per stations 1 and 2 in figure 1. Data was obtained from a polar array of 1800 sample points, evenly distributed over 18 radii ranging from 0.547m to 5.2m.

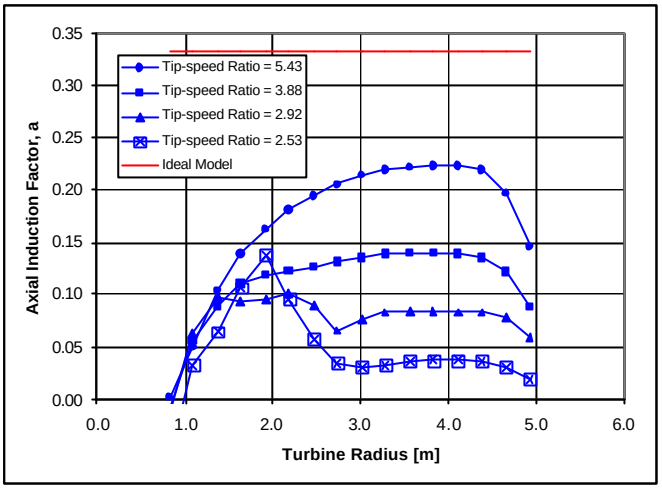

Figure 14. Axial Induction Factor compared against Ideal Actuator Disk model

The rotor plane axial velocity, *V*, was obtained by averaging the axial velocities V_1 and V_2 at the sample planes. By utilizing equation 7 a distribution of the axial induction factor, *a*, was measured over the turbine swept area. Since the data was evenly arranged over concentric circles, averaging each sample circle produced a resultant measure of *a* with respect to the turbine radius. The results for four operating points are illustrated in figure 14.

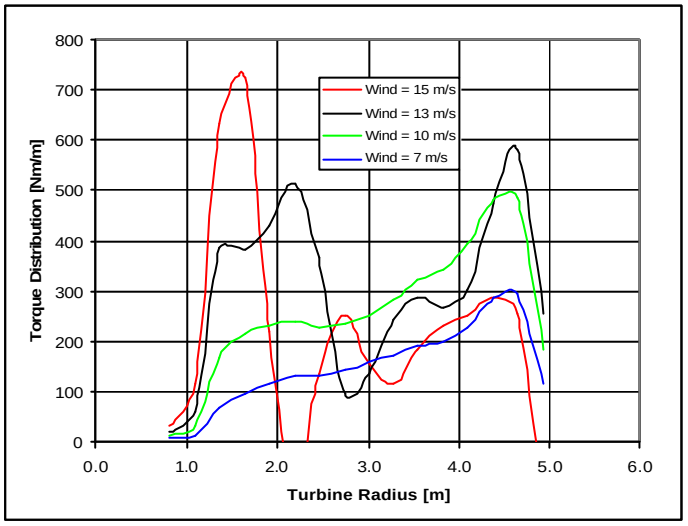

Figure 15. Torque Distribution calculated from the measured angular induction factor

The angular velocities in the flow were similarly sampled at stations 1 and 2. The rotor plane angular velocity, *?*, was obtained by averaging these values. Substituting the results into equation 11 produced a distribution of the angular induction factor. Utilising equation 12, the radial distribution of torque over the swept area was determined and results plotted in figure 15 for the four operating conditions tested.

Integrating the torque correlation with radius provides the total torque output from the actuator disk model. Results were compared against the experimental data and full turbine 3D model (figure 16). The plot shows a good match, except for the 15 m/s wind speed case. It is not clear why the agreement deteriorates at this condition.

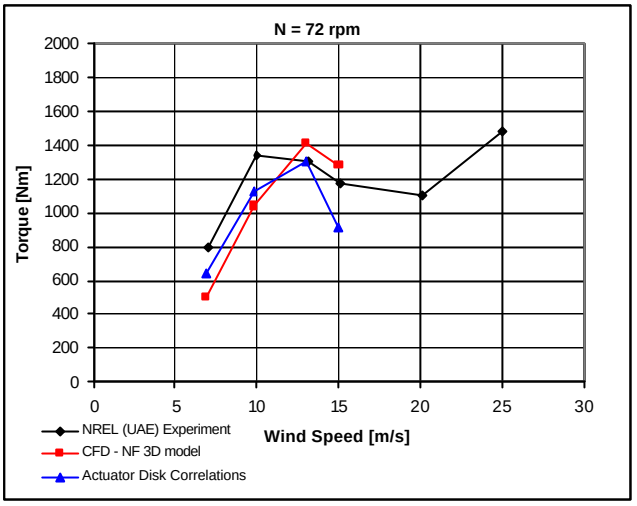

Figure 16. Torque Distribution calculated from the measured angular induction factor

The result verifies that, at least in the vicinity of the turbine peak efficiency point, an equivalent actuator disk model could potentially offer a cost-effective representation of a wind turbine. A full 3D turbine model is still required at selected operating conditions to extract the necessary induction factors. However, with an equivalent calibrated actuator model the turbine could be placed in larger environments or turbine array to assess in-situ performance. The follow-on work programme aims to explore this methodology in further detail.

6.0 Conclusions

The validation of CFD against 2D blade sections showed that using a high resolution structured mesh, with advanced turbulence and transition models provides an excellent match with experimental data in the attached flow regime. However, the CFD and XFOIL panel code over-predict peak lift and tend to underestimate stalled flow. Furthermore, utilising the same high fidelity model for a 3D case generates an extremely computationally demanding and expensive simulation.

Validation of a normal fidelity model of the 2D blade section showed a poor match in the attached flow regime, but better performance than the high fidelity model beyond the peak lift point. The UAE turbine blade operates over a complete range of aerofoil conditions, due to the use of tip-stall over-speed protection. Therefore, the normal fidelity model offered overall comparable performance with the high fidelity model, but at a significant saving in computational power and expense. The 3D results compared well with experiment over four operating conditions.

Results from the 3D benchmark exercise were used to calibrate Glauert's momentum actuator disk model. The axial and angular induction factors were determined using area averaged data sampled from upstream and downstream planes close to the turbine. The corresponding calculated torque output showed good agreement with the 3D CFD model and experimental data. However, for high wind cases the actuator model tended to diverge from the CFD results and experiment.

The results from this initial stage of work support the use of a calibrated actuator disk methodology based on a normal fidelity CFD modelling approach. Implementing actuator momentum correlations obtained from an equivalent CFD analysis offers a potentially

economical methodology for simulating complete multiple wind turbines within a specific environment.

References

[1] Jonkman, J.M., 2003, "Modelling of the UEA Wind Turbine for Refinement of FAST_AD," Technical report for the National Renewable Energy Laboratory, TP-500-34755

[2] White, F.M., 1988, *Fluid Mechanics*, 2nd Edition, McGraw-Hill, Singapore

[3] Madsen, H.A., Mikkelsen, R., Øye, S., Bak, C., and Johansen, J., 2007, "A Detailed Investigation of the Blade Element Momentum (BEM) model based on analytical and numerical results and proposal for modification of the BEM model," The Science of Making Torque from Wind, Journal of Physics: Conference Series 75

[4] Gorban, A. N., 2001, "Limits of the Turbine Efficiency for Free Fluid Flow," Journal of Energy Resources Technology, Vol. 123, pp. 311 – 317

[5] Simms, D., Schreck, S., Hand, M., and Fingersh, L.J., 2001, "NREL Unsteady Aerodynamics Experiment in the NASA-Ames Wind Tunnel: A Comparison of Predictions to Measurements," Technical report for the National Renewable Energy Laboratory, TP-500-29494

[6] Corbus, D., 2005, "Comparison between Field Data and NASA Ames Wind Tunnel Data," Technical report for the National Renewable Energy Laboratory, TP-500-38285

[7] Wolfe, W.P., and Ochs., S.S., 1997, "CFD Calculations of S809 Aerodynamic Characteristics," American Society of Mechanical Engineers wind energy symposium, Reno, NV (United States)

[8] Laursen, J., Enevoldsen, P., and Hjort, S., 2007, "3D CFD Quantification of the Performance of a Multi-Megawatt Wind Turbine," The Science of Making Torque from Wind, Journal of Physics: Conference Series 75

[9] Mikkelsen, R., 2003, "Actuator Disk Methods Applied to Wind Turbines," Dissertation submitted to Technical Uni. of Denmark, Fluid Mechanics, Dept. of Mech. Eng.